University of Groningen

Ventricular Zone Disruption in Human Neonates With Intraventricular Hemorrhage

McAllister, James P.; Guerra, Maria Montserrat; Ruiz, Leandro Castaneyra; Jimenez, Antonio J.; Dominguez-Pinos, Dolores; Sival, Deborah; den Dunnen, Wilfred; Morales, Diego M.; Schmidt, Robert E.; Rodriguez, Esteban M.

IMPORTANT NOTE: You are advised to consult the publisher's version (publisher's PDF) if you wish to cite from it. Please check the document version below.

Document Version
Publisher's PDF, also known as Version of record

Link to publication in University of Groningen/UMCG research database

ORIGINAL ARTICLE

Ventricular Zone Disruption in Human Neonates With Intraventricular Hemorrhage

James P. McAllister, PhD, Maria Montserrat Guerra, PhD, Leandro Castaneyra Ruiz, PhD,
Antonio J. Jimenez, PhD, Dolores Dominguez-Pinos, MD, PhD, Deborah Sival, MD,
Wilfred den Dunnen, MD, PhD, Diego M. Morales, MS, Robert E. Schmidt, MD, PhD,
Esteban M. Rodriguez, MD, PhD, and David D. Limbrick, MD, PhD

Abstract

To determine if ventricular zone (VZ) and subventricular zone (SVZ) alterations are associated with intraventricular hemorrhage (IVH) and posthemorrhagic hydrocephalus, we compared postmortem frontal and subcortical brain samples from 12 infants with IVH and 3 nonneurological disease controls without hemorrhages or ventriculomegaly. Birth and expiration estimated gestational ages were 23.0–39.1 and 23.7–44.1 weeks, respectively; survival ranges were 0–42 days (median, 2.0 days). Routine histology and immunohistochemistry for neural stem cells (NSCs), neural progenitors (NPs), multiciliated ependymal cells (ECs), astrocytes (AS), and cell adhesion molecules were performed. Controls exhibited monociliated NSCs and multiciliated ECs lining the ventricles, abundant NPs in the SVZ, and medial vs. lateral wall differences with a complex mosaic organization in the latter. In IVH cases, normal VZ/SVZ areas were mixed with foci of NSC and EC loss, eruption of cells into the ventricle, cytoplasmic transposition of N-cadherin, subependymal rosettes, and periventricular heterotopia. Mature AS populated areas believed to be sites of VZ disruption. The cytopathology and extension of the VZ disruption correlated with developmental age but not with brain hemorrhage grade or location. These results corroborate similar findings in congenital hydrocephalus in animals and humans and indicate that VZ disruption occurs consistently in premature neonates with IVH.

Key Words: Astrocytes, Ependyma, Intraventricular hemorrhage, Neural stem cells, Posthemorrhagic hydrocephalus, Subventricular zone, Ventricular zone.

From the Department of Neurosurgery, Washington University School of Medicine, St Louis, Missouri (JPM, LCR, DMM, DDL); Instituto de Antomía, Histologia y Patologia, Facultad de Medicina, Universidad Austral de Chile, Valdivia, Chile (MMG, EMR); Instituto de Biología Celular, Genética y Fisiología Facultad de Ciencias, Universidad de Malaga, Malaga, Spain and Instituto de Investigación Biomédica (IBIMA), Malaga, Spain (AJJ, DDP); Departments of Pediatrics, Pathology and Medical Biology, University Medical Center Groningen, University of Groningen, Groningen, The Netherlands (DS, WD); Department of Pathology and Immunology, Washington University School of Medicine, St Louis, Missouri (RES); and Department of Pediatrics, Washington University School of Medicine, St Louis, Missouri (DDL)

Send correspondence to: James P. McAllister, PhD, Department of Neurosurgery, Washington University School of Medicine, 425 S. Euclid, Campus Box 8057, St Louis, MO; E-mail: pat.mcallister@wustl.edu

James P. McAllister and Maria Montserrat Guerra contributed equally to this work as co-first authors.

Esteban M. Rodriguez and David D. Limbrick contributed equally to this work as co-senior authors.

INTRODUCTION

Intraventricular hemorrhage (IVH) is the most common neurological complication of preterm birth (1–3) and up to 50% of IVH patients develop posthemorrhagic hydrocephalus (PHH) (4–9). The risk of developing PHH is higher in more severe grades of IVH (grades 3 and 4), the frequency of IVH admissions is increasing, and hospital length of stay and average cost per patient has been trending upward since 2000 (10, 11). Long-term treatment usually consists of surgical diversion by catheter shunting of cerebrospinal fluid (CSF) from the cerebral ventricles to alternative absorption sites or endoscopic third ventriculostomy with or without choroid plexus cauterization. Nevertheless, even after surgical treatments that reduce intracranial pressure and ventriculomegaly to varying degrees, PHH is still associated with debilitating neurological sequelae and a 3- to 4-fold increase in cognitive and psychomotor disabilities (4, 12). Attentional and academic deficits exist even in school-age children born preterm with apparent arrested hydrocephalus (13). Consequently, IVH and PHH are

important neurological conditions with significant neurological impairments and suboptimal clinical treatments.

In spite of the prevalence and poor outcome of PHH, the pathogenesis of this disorder is poorly understood (14, 15). The traditional perspective often focuses on the blockage of CSF flow and absorption pathways by blood and blood products (16, 17), leaving the pathophysiology to include only the secondary effects of ventriculomegaly and raised intracranial pressure. Recently, however, evidence from both experimental (18–27) and clinical (18, 28–32) studies of congenital hydrocephalus, including fetal and perinatal models of ciliopathies (33–6), indicates that there may be other mechanisms that contribute to the development of PHH, including the loss of multiciliated ependyma (18). A series of studies on hyh (hydrocephalus with hop gait) mice, which develop aqueduct stenosis during the perinatal period, have supported the concept of a genetic defect in the cell junction complexes of the cells forming the ventricular zone (VZ) (20, 24–6, 37–41). Following nomenclature used in Bystron et al (42), namely, the multipotent radial glia/stem cells, hereafter called neural stem cells (NSCs), present in early and mid-developmental stages; ependymal cells (ECs) occur in the perinatal period. The genetic defect results in the disassembling and loss of these cells. This phenomenon was first described as ependymal denudation (39) and later designated as VZ disruption. In addition, recent studies of CSF proteins by Limbrick et al suggest that alterations in cell adhesion molecules such as L1-cell adhesion molecule, brevican, and neural cell adhesion molecule-1 occur in perinatal human hydrocephalus (43, 44).

Several studies have demonstrated that VZ disruption, loss of NSCs into the CSF, exposure of neural progenitor (NP) cells of the subventricular zone (SVZ), abnormal migration of neuroblasts and periventricular heterotopia (PH) occur in fetuses with hydrocephalus and spina bifida (18, 27, 32, 37, 45). Krueger et al (46) reported the presence of NP cells in the CSF of preterm infants with PHH, which strongly supports the possibility that in these patients there is a disruption of the VZ. A few studies have examined the VZ in humans following IVH (16). Fukumizu et al (47, 48) described EC loss and subependymal rosette formation in children with fetal and neonatal PHH but their observations were restricted to the cerebral aqueduct and fourth ventricle. The present investigation was aimed to test the hypothesis that VZ disruption and its outcomes, that is, loss of NSCs and ependyma denudation, occur in the telencephalon of infants with IVH of prematurity.

MATERIALS AND METHODS

Subjects and Specimens

Autopsy specimens from preterm infants diagnosed with IVH were obtained from the St Louis Children's Hospital (SLCH) at the Washington University School of Medicine, St Louis, MO (n = 10), the University Medical Center Groningen, University of Groningen, Groningen, Netherlands (n = 1), and the Regional Clinical University Hospital of Malaga, Malaga, Spain (n = 2). Control cases (n = 3), defined as preterm infants with no intracerebral hemorrhage or ventriculomegaly who expired from nonneurological causes, were obtained from SLCH. Twelve control human fetuses ranging in age between 16 and 40 gestational weeks (GW), studied in a previous investigation (18), were also considered to reinforce the present investigation. The ages of all patients were estimated from the time of expected fertilization and recorded as estimated gestational age (EGA). Routine clinical and diagnostic observations were available from the hospital records. The human subjects research committees of the respective institutions waived or approved all procedures.

Neuroimaging

Patients at SLCH (but not Groningen and Malaga) had undergone routine head ultrasound (US) examinations to screen for IVH and identify IVH grades following the classification of Papile et al (49) and the descriptions of Volpe et al (49, 50). Briefly, these classifications were based on the following features: Grade 1 (IVH-1), parenchymal/subependymal hemorrhage with <10% involvement of the ventricle; Grade 2 (IVH-2), IVH involving 10%–50% of the ventricles but with no ventriculomegaly; Grade 3 (IVH-3), IVH involving >50% of the ventricles with ventriculomegaly; and Grade 4 (IVH-4), ventricular and parenchymal hemorrhage (hemorrhagic infarction) with ventriculomegaly. Frontal-occipital horn ratios were obtained from US images to quantify ventricular sizes following published methods (51).

TABLE 1. Cell Types of the VZ in Human Fetuses

Cell Type	Function	Basal Process	Cilia	Immuno-histochemical Markers	Predominant Ventricle Wall Location[a]	Figures
1	Uncommitted NSC[b]	Long radial	One	GFAP+, AQP 4+, βIV-tub-	Lateral and dorsal	2, 7, Sup 2–5
2	Early pre-ependymal NSC	Long radial	One	GFAP+, βIV-tub+	Lateral and dorsal	7, Sup 2, 3
3	Late pre-ependymal NSC	Long radial	One	GFAP-, βIV-tub+	Lateral and dorsal	2, 7, Sup 3
4	Committed early ependyma	Short	None	GFAP+, βIV-tub+	Lateral and medial	6, 7, Sup 2
5	Immature ependyma	Short	Multi	GFAP+, βIV-tub+	Medial	6, Sup 2–5
6	Immature ependyma	Short	Multi	GFAP−, βIV-tub+	Medial	6, 7, Sup 4
7	Mature ependyma	None	Multi	GFAP−, βIV-tub+	Medial	7, Sup 5

[a]During the second half of gestation.
[b]NSC, also regarded as radial glia.
GFAP+, glial fibrillary acidic protein-positive; βIV-tub+, βIV-tubulin-positive. βIV-tubulin is a component of the cilium microtubules. Sup, Supplementary Data figures.
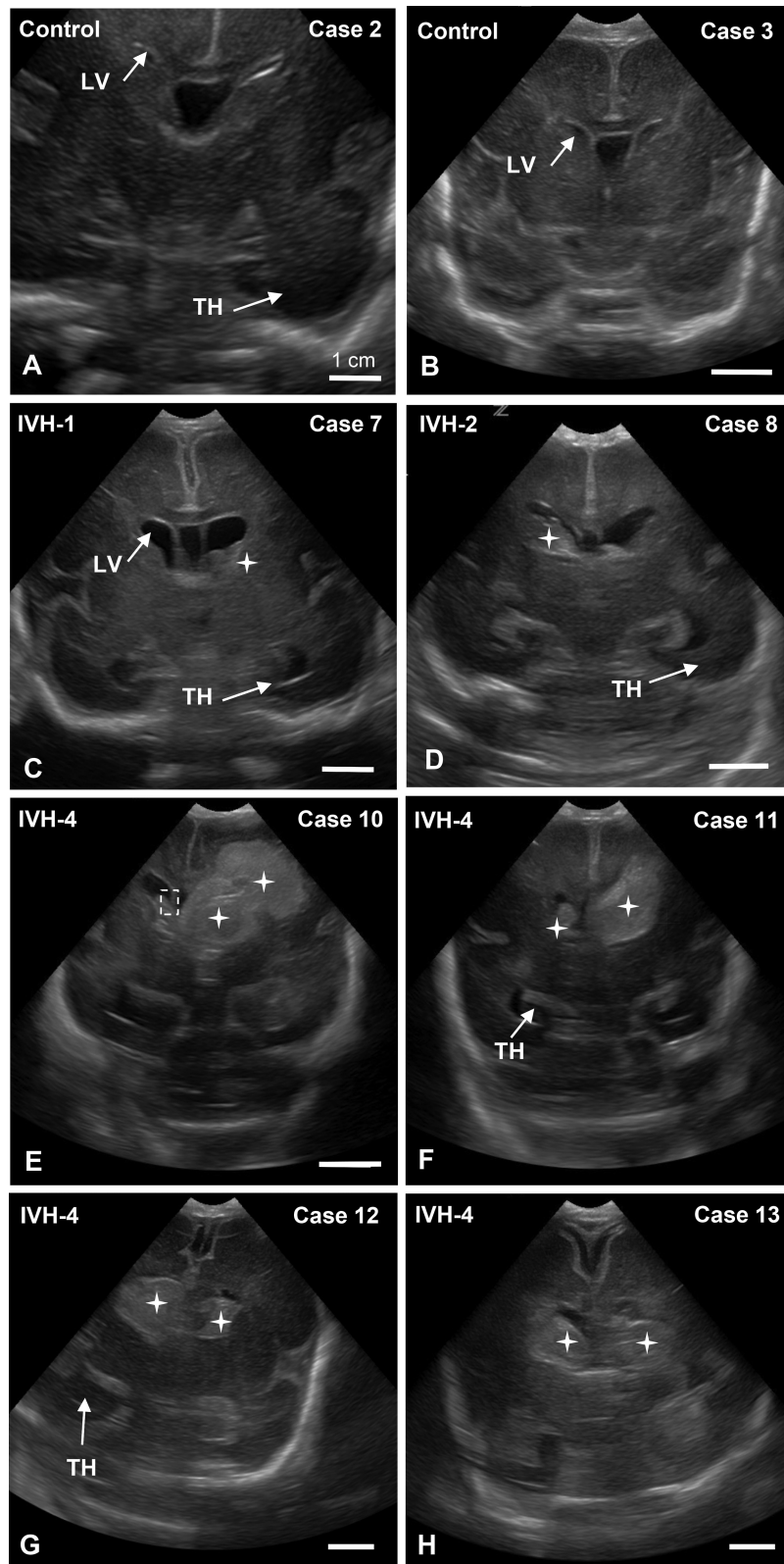
FIGURE 1. US images of coronal sections showing the appearance of normal LVs in control infants **(A, B)** and preterm infants with IVH grades 1 **(C)**, 2 **(D)**, and 4 **(E–H)**. Hemorrhages are outlined or identified by stars; the dashed-line rectangle in **E** delineates the region shown in Supplementary Data Figure S2A–F'. Scale bars = 1 cm.

TABLE 2. Case Histories Listed by Increasing IVH Scores

Case no.	Condition	EGA birth in weeks	Survival in days	US days postbirth	HMG, days duration	FOHR	Neuropathologic Findings from Clinical Records[a]
1	Control	23 3/7	0	NA	None	NA	No HMG, PDA, PFO, abnormal lobation right and left lung, large right pneumothorax, no gross brain abnormality, placental abruption likely the cause of all pathology
2	Control	24	0	NA	None	0.50	No HMG, subpulmonary pneumothorax
3	Control	25 1/7	8	NA	None	0.49	Sepsis, normal brain, severe mixed respiratory and metabolic acidosis
4	IVH-1	27 5/7	12	10	2–12	0.48	Germinal matrix/parenchymal HMG
5	IVH-1	35	32	9 and 29	28–32	0.40	Abnormal karyotype, initial IVH-1, small right subependymal hemorrhage, later normal on US
6	IVH-1	38 1/7	41	8 and 42	37–45	0.44	HIE, initial IVH-1 later normal
7	IVH-1 or 2	28	2	1 and 2	1–2	0.43	402 Kb maternally inherited interstitial deletion on chromosome 12p, diffuse lung injury, pneumopericardium, blood filled cystic right chest wall mass, subependymal and unilateral CP HMG, lymphatic venous malformation = COD, mild dilation posterior horn LV, mild reactive gliosis, periventricular calcifications could be infections
8	IVH-2	23 3/7	1	0	1	0.48	Massive pulmonary HMG, hyaline membrane disease, sepsis
9	IVH-3	29 4/7	14	2	3–16	0.46	HIE, bilateral HMG and small SAH, mild ventriculomegaly
10	IVH-4	23	5	3	2–5	0.57	Respiratory failure, focal acute pneumonia right lung, PDA, PFO
11	IVH-4	24	2	2	0–2	0.50	Diffuse pulmonary HMG = COD, PFO, coagulopathy, subependymal HMG, intracranial bleed
12	IVH-4	27 6/7	1	NA?	0–1	0.39	Hyaline membrane disease, pulmonary insufficiency, rest of body normally formed, COD = pulmonary consolidation, PFO, IVH in all ventricles
13	IVH-4	28	19	6	13–19	0.53	Respiratory failure and IVH4 = COD, Beckwith-Wiedemann Syndrome, PDA
14	IVH-4	NA	NA	NA	NA	NA	Hemodynamic failure = COD. Subependymal HMG in left hemisphere and a massive IVH, IVH-4 determined by neuropathologist; Malaga
15	IVH-4	26 1/7	6	NA	0–6	NA	PHH; IVH-3 and 4 in left and right LVs, respectively; periventricular venous infarction; Groningen
16	IVH-4	23	0	NA	NA	NA	IVH-4 determined by neuropathologist; Malaga
17	SAH	39 1/7	0	NA	No IVH	NA	Diffuse pulmonary HMG, systemic hypoxia, transposition of great vessels, PDA, PFO, occipital SAH, skull and fontanels normal, cortical convolutions, and SC normal

[a]All from SLCH unless indicate for Groningen and Malaga.

CP, choroid plexus; COD, cause of death; EGA, equivalent/estimated gestational age from menstrual cycle; e.g. 23 3/7 = 23 weeks + 3 days; FOHR, frontal-occipital horn ratio; HIE, hypoxia/ischemia; HMG, hemorrhage; IVH, intraventricular hemorrhage (diagnosed by US); LV, lateral ventricle; NA, not available; PDA, patent ductus arteriosis; PFO, patent foramen ovale; SAH, subarachnoid hemorrhage; SC, spinal cord; US, ultrasound.

Tissue Processing and Immunohistochemistry

Brain specimens were dissected from regions of the frontal cortex containing the frontal horn of the lateral ventricle (LV) and adjacent cortical and subcortical areas, including the ganglionic eminence (GE). Following fixation in 10% formaldehyde in phosphate buffer or Bouin's solution (as soon as possible following patient death), these specimens were embedded in paraffin and sectioned serially at 15 μm using routine methods. Sections were stained with hematoxylin and eosin (H&E) to visualize cytoarchitecture and confirm the location of the VZ and SVZ. Adjacent sections were processed for double immunofluorescence using antibodies to the following in pairs: 1) βIII-tubulin (1:750, mouse monoclonal Sigma, St Louis, MO); 2) βIV-tubulin (1:50, mouse monoclonal, Abcam, Cambridge, UK); 3) glial fibrillary acidic protein ([GFAP], 1:750, rabbit polyclonal, Sigma); 4) N-cadherin (1:50, rabbit monoclonal, Santa Cruz Biotechnology, Inc., Dallas, TX); and 5) aquaporin-4 (1:750, rabbit polyclonal, Abnova, Heidelberg, Germany). Appropriate secondary antibodies conjugated with Alexa Fluor 488 or 594 (1:500; Invitrogen, Carlsbad, CA) were used. Antibodies were diluted in a buffer containing 0.1 mol/L Tris buffer, pH 7.8, 0.7% nongelling seaweed gelatin, lambda carrageenan, and 0.5% Triton X-100 (Sigma). Incubation was carried out for 18 hours at room temperature. Omission of the primary antibody during incubation provided the control for the immunoreactions.

Light Microscopy

Sections were studied under epifluorescence using the multidimensional acquisition software AxioVision Rel (version 4.6) of Zeiss (Aalen, Germany) or by confocal
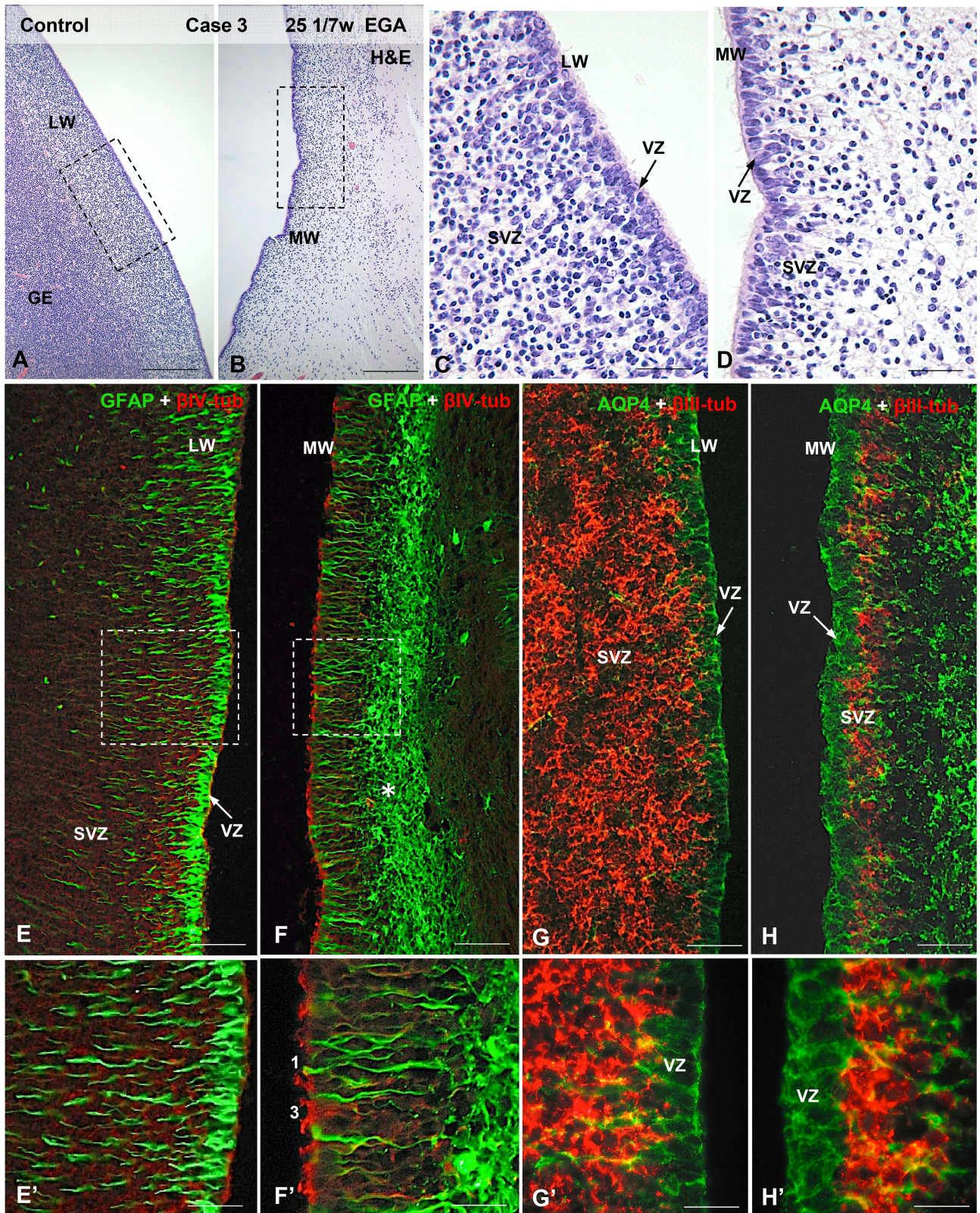
FIGURE 2. Photomicrographs from Case 3 (see Fig. 1B) illustrating the cytology and cytoarchitecture of the VZ and SVZ zones in control brains. **(A)** LW of the LV containing the GE; H&E staining. **(B)** MW of the LV. **(C, D)** Detailed magnification of the areas framed in (A) and (B) showing the distinct cytological characteristics of the lateral (C) and medial (D) ventricular walls. **(E–H)** In the lateral ventricular wall the VZ is formed by GFAP-positive **(E, E')** and AQP4-positive **(G, G')** NSCs, and the thick SVZ contains

microscopy (Zeiss LSM700) with the acquisition software Zen 2012.

Because the developmental progression of ependymal and progenitor cells in the VZ is dynamic, a classification of cell types was devised based on the literature (42, 52–7) and our personal observations of the specimens. Cell types were identified within the VZ (immediately adjacent to the ventricle), which are believed to follow a developmental progression from least- to most-differentiated (Table 1; Figs. 1, 6, 7; Supplementary Data Figs. S2–S6, S7). Type 1 cells have the phenotype of NSCs (long radial process, primary cilium, expression of GFAP and AQP4); because they express neither βIII-tubulin (neuronal lineage) or βIV-tubulin (ependymal lineage), they most likely correspond to uncommitted NSCs. The co-expression of GFAP and βIV-tubulin in monociliated cells with a long radial process (type 2 cells) suggests they are NSCs committed to the ependymal lineage. The progressive shortening of the radial process (and consequently loss of contact with the external limiting membrane of the brain) of βIV-tubulin-positive cells and the progressive appearance of multiple cilia would reflect a continuum from types 3–6 cells, culminating with the multiciliated cylindrical βIV-tubulin-positive, AQP4-positive cells (type 7) that correspond to mature ependyma. Other progenitor cells in the SVZ, predominantly the so-called intermediate progenitor cells that give rise to neural and glial cells during fetal, postnatal and adult stages, were not individually distinguished.

RESULTS

Human Cases

This study was conducted on 17 patients summarized in Table 2. Controls (Cases 1–3) were patients with no IVH or ventriculomegaly who expired acutely from nonneurological causes. Twelve control human fetuses 16 and 40 EGA from a previous investigation (18) gave further support to this study. IVH was clearly demonstrated at one or more time points in 13 cases; of these, 3 were classified as IVH-1 (Cases 4–6). Cases 5 and 6 were initially diagnosed with IVH-1 but 33 and 45 days later, respectively, were judged by US to have no IVH or ventriculomegaly; nevertheless, because IVH had occurred at some time during gestation these cases were included in the IVH-1 group. One case exhibited IVH-1 or IVH-2 (Case 7) and one clearly had IVH-2 (Case 8). One case had IVH-3 (Case 9). Nine cases exhibited IVH-4 (Cases 10–16). Case 15 was graded as IVH-3 and IVH-4 from the left and right LVs, respectively; nevertheless, since IVH-4 occurred in at least a portion of the ventricles this case was included in the IVH-4 group. Case 17 had a subarachnoid hemorrhage (SAH) at birth (39 1/7 EGA), but the skull, anterior fontanelle, cortical convolutions and spinal cord were all unaffected; and no hemorrhage was reported in the cerebral ventricles.

Birth (as determined by the EGA) of the 3 controls was at ~23–24 weeks and survival was 0–8 days (median, 0). Combining the IVH-1 and IVH-2 cases, birth occurred either relatively early preterm at ~23–28 EGA weeks in 3 cases (Cases 4, 7, and 8) or late preterm at ~35 or 38 EGA weeks in 2 cases (Cases 5 and 6). These "early" and "late" groups survived 1–12 days (median, 2.0 days) and 33–42 days (median, 37.5 days), respectively. Combining the IVH-3 and 4 cases, birth occurred relatively early at ~23–30 EGA weeks (median 26 weeks) and survival was 0–19 days (median, 1.5 days).

As in clinical care, the exact time of the hemorrhagic episode cannot be precisely determined. To estimate the approximate time elapsed between hemorrhage and death, we considered the date of birth, date of the US, and the date of death. For each case, a range of time for the hemorrhage-to-death period was estimated, where the US-to-death period was the shortest and the birth-to-death period was the longest. This estimate was also influenced by the fact that 90% of IVH incidents occur within 72 hours after birth, with half of them occurring in the first 24 hours (58, 59).

It should be noted that often the cause of death (Table 2) was related to systemic failure, for example, cardiac abnormalities or failure, or pulmonary complications (hemorrhage, respiratory failure, hyaline membrane disease).

Neuroimaging

Cases 1–13 and 15 received an US diagnosis during the first week after birth to grade IVH and assess the morphological appearance of the brain (Table 2). Cases 14 and 16 were judged to be IVH-4 based on the neuropathology evaluation. Figure 1 illustrates the representative US appearance of control brains (Fig. 1A, B) and the changes that occur with different grades of IVH. IVH-1 and IVH-2 brains exhibited no or minimal ventriculomegaly, with the hemorrhage contained within the lateral wall (LW) of the frontal horns of the LV, usually involving the GE (Fig. 1C, D). Large hemorrhages always occupied the ventrolateral walls of the LVs and blood usually filled the frontal horns in IVH-4 cases (Fig. 1E–H).

VZ and SVZ Cytology in Control Brains and Nonaffected Regions of IVH Brains

The normal cell organization and the cell lineages forming the VZ and the internal subventricular zone (iSVZ) and outer (oSVZ) SVZs (Fig. 3B') of the telencephalon exhibited large variations throughout development and along distinct regions of the MW, LW and dorsal walls (DWs) of the LVs (Fig. 2B). The control cases with EGAs between 23 and 25 GW exhibited normal VZ and SVZ morphology, as previously described (18, 52–4, 60). Three cell types, all considered to be NSCs and ECs in different stages of maturation (Table 1),

FIGURE 2. Continued

βIII-tubulin-positive neural precursor cells (**G, G'**). In the medial ventricular wall the VZ is formed by a mixed population of GFAP-positive (**F, F'**, type 1) and AQP4-positive (**H, H'**) NSCs and βIV-tubulin-positive multiciliated cells (**F, F'**, type 2,); the slender SVZ contains a few βIII-tubulin-positive neural precursor cells (**H, H'**). A thick network of AS underlies the SVZ (**F, H**, asterisk). Scale bars: **A, B**, 300 μm; **C, D**, 50 μm; **E-H**, 100 μm; **E'-H'**, 25 μm.
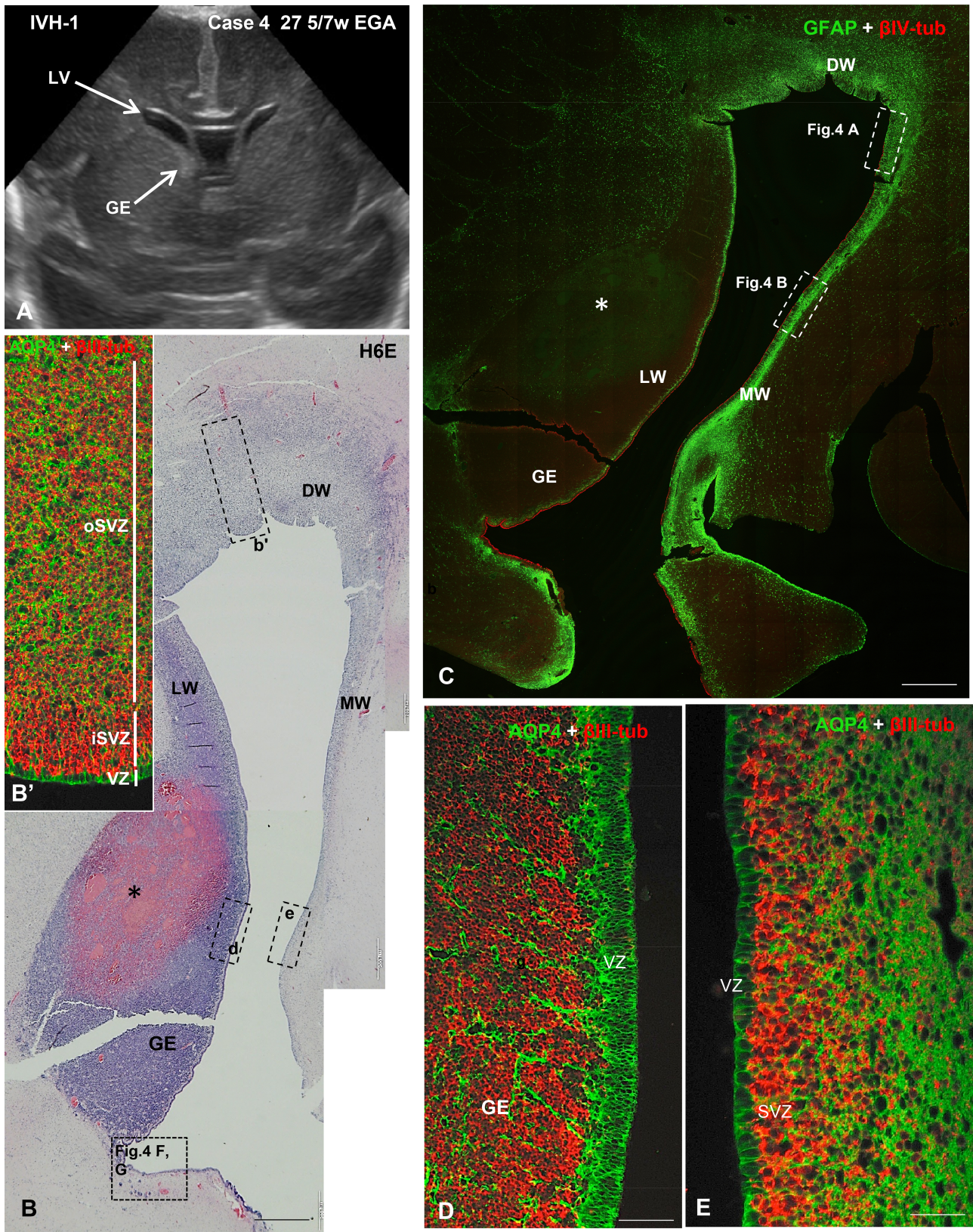
FIGURE 3. US image and photomicrographs from Case 4 illustrating the cytology and cytoarchitecture of the VZ typically found in IVH-1 cases. **(A)** A coronal US taken 2 days before death showing relatively small LVs and a prominent GE in the lateral wall of the frontal horn. **(B)** A H&E-stained section through the LW, MW, and dorsal (DW) walls of the LV showing a large hemorrhage

were found in the VZ of the control cases and in the nonaffected regions of the ventricular walls of 23–27 GW IVH cases (Fig. 2): Type 1 cells had a long radial process expressing AQP4 in the plasma membrane domain and GFAP throughout the cytoplasm and projected a single cilium. Type 2 cells were similar to type 1 cells but they expressed both GFAP and βIV-tubulin in their cytoplasm. Type 3 cells exhibited a basal process and expressed βIV-tubulin throughout the cytoplasm but not GFAP (Figs. 2E–H', 7G; Supplementary Data Fig. S2F).

In 23–25 GW preterm infants, the VZ of the medial wall (MW) was formed by intermingled populations of cell types 1–3 (Fig. 2B, D, F', and H'). The iSVZ was occupied by βIII-tubulin-positive NP cells clustered in between the basal processes of the NSCs (Fig. 2H, H'; Supplementary Data Fig. S2A–D). The oSVZ was a loose layer of βIII-tubulin-positive cells intermingled with radial glial-type cells expressing AQP4 in the plasma membrane domain and GFAP in the cytoplasm (Supplementary Data Fig. S1A–D). In the LW, the VZ was exclusively formed by type 1 cells (NSC) (Figs. 1E, E', G, and G'). The density of βIII-tubulin-positive NP cells in the iSVZ was similar to that on the MW but the extent of the oSVZ was much larger than that of the MW (Supplementary Data Fig. S1A, B).

VZ and SVZ Cytology in IVH Cases

In all cases of IVH, irrespective of the grade and location of hemorrhage, intermittent portions of the VZ exhibited disruption. In the sections of frontal horn examined, the cytopathology and extent of VZ disruption appeared to be associated with developmental age and not to the degree or location of the brain hemorrhage. In all cases, the disruption affected circumscribed regions of the ventricular walls, with the nonaffected regions displaying a similar cell organization as was seen in the controls. In most cases, the VZ pathology occurred in the LW of the ventricles. For descriptive purposes, the IVH cases will be separated into three developmental groups based on the EGA at birth (in GW), rounded to the nearest full week for simplicity.

23–27 GW IVH: Cases 4 (IVH-1), 8 (IVH-2), 10 (IVH-4), 11 (IVH-4), 15 and 16 (IVH-4)

Most of the VZ/iSVZ of the medial and LWs of the LVs were not affected (Figs. 3D, E, and 4D). At these developmental ages, the cell organization of the lateral and MWs was identical to that of the 23–24 GW control cases.

The VZ of the lateral and DWs was exclusively formed by type 1 cells (Fig. 3B–D; Supplementary Data Fig. 1E, F). The iSVZ was formed by βIII-tubulin-positive NP cells densely packed between the long radial processes of the NSCs (Fig. 3B, B', D; Supplementary Data Fig. S1B, E, F). The oSVZ was an extended layer of loosely arranged βIII-tubulin-positive cells intermingled with NSCs expressing AQP4 and GFAP (Fig. 3B'; Supplementary Data Fig. S1A, B). The VZ of the MW was formed by a mixed population of cell types 1–5 (Supplementary Data Fig. S1I). The SVZ was formed by a layer of densely packed βIII-tubulin-positive NP cells (Fig. 3E; Supplementary Data Fig. S1B–D).

There were distinct alterations in the cell organization of the VZ/iSVZ in the affected areas. These included: 1) very small areas (about 25 μm across) involving the disruption of a few RG cells resulting in exposure of NP cells to the ventricular CSF (Figs. 4B–C', 7B, C; Supplementary Data Fig. S1E–F'); 2) small areas (∼50–100 μm across) in which the lost VZ was occupied by numerous NP cells and a few astrocytes (AS) (Figs. 5C–C'', 7C, C'); 3) small areas (about 100 μm across) in which the disrupted VZ was replaced by a patch of GFAP-positive/AQP4-positive AS, appearing to prevent the underlying NP cells from reaching the ventricle (Figs. 4B–C', E, 7D, D'); 4) large denuded areas (∼500 μm in length) endowed with a layer of AS (Figs. 4A, 5A''–B''', 7F, F'; Supplementary Data Fig. S5A); and 5) PH of ∼30–60 μm in diameter found close to the ventricle. They were formed by βIII-tubulin-positive cells surrounded by a nest of AS (Figs. 4F, G, 7J). All or most of the 5 abnormalities could be found in each case (see Cases 4 and 15 in Figs. 3–5).

28-32 GW IVH Cases: Cases 7 (IVH-1/2), 9 (IVH-3), 12–14 (IVH-4)

In nonaffected regions at these gestational ages, the cell organization of the medial and LWs of the ventricle changed in comparison to the younger preterm infants. In Case 7 (28 GW; Supplementary Data Figs. S2, S3), the VZ of the MW was formed by GFAP-positive cells with a short basal process and no cilia (type 4), GFAP-positive cells with a short basal process and βIV-tubulin-positive cilia (type 5), GFAP-negative cells with a short basal process and βIV-tubulin-positive cilia (type 6) and GFAP-negative, βIV-tubulin- nonciliated cells (Figs. 6B–B'', 7H, H'; Supplementary Data Fig. 2C, C') whereas the VZ of the LW was mostly formed by a mixed population of type 1–5 cells (Supplementary Data Fig. S2F). In case 14, the MW was mostly formed by type 6 cells and the LW by a mixed population of types 4–6 cells (Fig. 6B–B'').

FIGURE 3. Continued

(asterisk) in the GE. Dashed-line boxes demarcate regions shown in **B' (b')**, **D (d)** and **E (e)** of this figure, as well as in Figure 4F, G. **(B')** Area similar to that framed in **b'**, immunostained for AQP4 and βIII-tubulin. The VZ, iSVZ and oSVZ zones are shown. **(C)** Section adjacent to that of panel **B**. Double immunofluorescence for GFAP (green) and βIV-tubulin (red) showing the distinct cytoarchitecture of the LW, MW, and DW ventricular walls. The areas framed are shown in Figure 4A, B. A thick network of GFAP-positive AS underlies the SVZ of the MW. **(D)** In the LW of the frontal horn of the LV (the dashed-line box in the inset **d** of panel **B** shows the location) the GE is prominent and filled with neural progenitor cells (NPCs) immunostained with βIII-tubulin; stem cells in the VZ are intensely stained with AQP4. **(E)** In the MW of the LV (the dashed-line box in the inset e of panel B shows the location), the AQP4-positive stem cells extend processes into the SVZ and βIII-tubulin-stained NPs can be seen migrating from the VZ. Scale bars: **B, C**, 600 μm; **C'**, 15 μm; **D, E**, 50 μm.
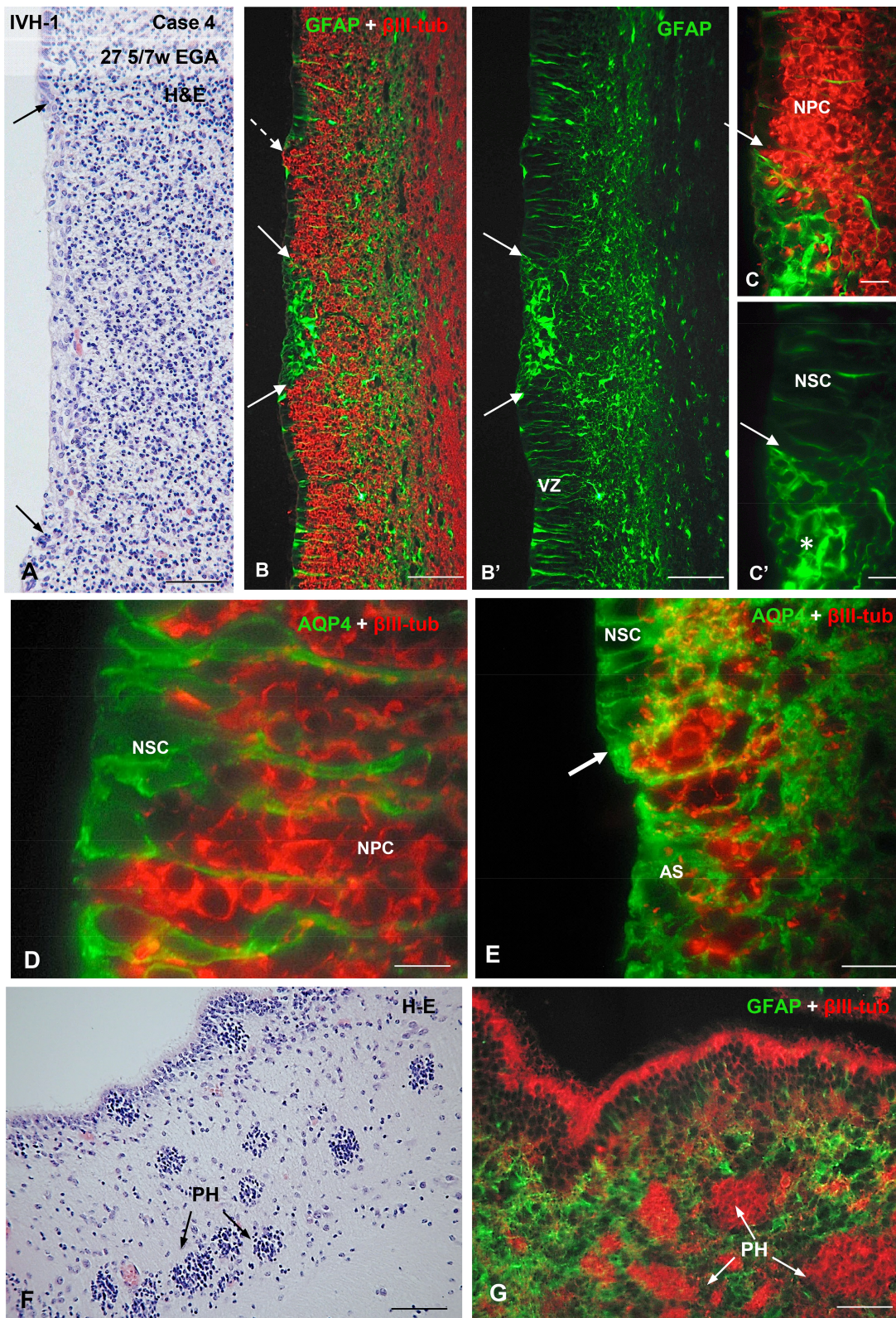
FIGURE 4. Photomicrographs from Case 4 at higher magnification illustrating the cytology and cytoarchitecture of the VZ typically found in this IVH-1 case. **(A)** Area of the MW of the LV similar to that demarcated in Figure 3C. H&E-stained section showing segment of disrupted VZ (between the arrows). **(B)** Magnification of another area of the MW framed in Figure 3C. Double immunofluorescence for GFAP (green) and βIII-tubulin (red) showing 1 site of VZ disruption (between solid arrows)

None of the 6 cell types expressed βIII-tubulin ([Figs. 3D, E, 4D, 7A, A']).

Alterations 1–4 described for the younger group of IVH cases (see above) were also found in the affected regions of the 28–32 GW IVH cases; however, in these older cases the frequency and size of the disruption foci were increased ([Fig. 6]; Supplementary Data Figs. S2A, B, D–F, S3A, SA'). The width of the disruption areas ranged between 30 μm to 500 μm. Cell types 1–5 were found at the disruption border, indicating that all of them were affected by the disruption (Supplementary Data Figs. S2E, F, S3A', C). At the disruption front there were type 1 cells that had AQP4 in the cytoplasm, in addition to the plasma membrane domain, suggesting that they might correspond to radial glial-type cells differentiating into AS (Supplementary Data Fig. S3B, B'). The existence in the same discrete region of multipolar GFAP-positive cells, with one of the processes reaching the ventricle, and the presence in the disrupted area proper of loosely arranged multipolar AS, also points to the possibility that AS re-populating the disrupted VZ originate locally (Supplementary Data Fig. S3C).

In one of the cases (Case 9, 31 GW, IVH-3, with bilateral IVHs), the disruption pathology was especially severe (Supplementary Data Fig. S4), with a large surface of the lateral and MWs of the frontal horn denuded (Supplementary Data Fig. S4A). In other regions of the LVs, the MW had a normal appearance, with the VZ formed by cell types 1–6 (Supplementary Data Fig. S4D, F). In sharp contrast, the opposite LW was completely disrupted, with radial glial-type cells and NP cells forming a "peninsula" of tissue protruding into the ventricle and covering portions of intact VZ and SVZ (Supplementary Data Fig. 4B–H).

35-39 GW IVH and SAH Cases: Cases 5 and 6 (IVH-1) and Case 17 (SAH)

In nonaffected regions there were mature multiciliated ependyma (type 7) and a few scattered NSC (type 1) comprising the entire VZ of the ventricular walls. In the LW, the iSVZ contained a thin layer of NP cells (Supplementary Data Fig. S5B–B'').

In the affected regions, most of the MW was denuded, with a few islands of ependyma resisting disruption (Supplementary Data Fig. S5A, C–C''). At variance, most of the LW was lined by ependyma with only small foci of VZ disruption. The denuded regions were occupied by a thick layer of densely packed AS (Supplementary Data Fig. S5A, inset, C,

C''). Close to the denuded areas there were ependymal rosettes formed by βIV-tubulin-positive cells joined together by N-cadherin-based junctions (Supplementary Data Fig. S5E, F, F'). Numerous PH, ranging in diameter between 75 and 150 μm, were observed at ∼1.5–2 mm distance from the ventricular wall (Supplementary Data Fig. S5A); these heterotopia were closely associated with large blood vessels and were formed by densely packed βIII-tubulin-positive spherical cells ∼10 μm in diameter (likely corresponding to neuroblasts), surrounded by a distinct nest of AS ([Fig. 7J]; Supplementary Data Fig. S5D, D').

N-Cadherin-Based Junctions: Case 14 (IVH-4) and Case 17 (SAH)

Because our previous observations had noted alterations in junction complexes ([18, 22]), immunohistochemistry for N-cadherin was performed. Two cases are illustrated: one represents IVH-4 (Case 14, [Fig. 6]) and another with only a SAH (Case 16, Supplementary Data Fig. S5). In the nonaffected regions of the ventricular walls, the VZ cells displayed N-cadherin as small patches located on the lateral plasma membrane ([Fig. 6C–D']). In contrast, cells at the border of the disrupted areas expressed N-cadherin as masses located in the cytoplasm ([Fig. 6D, D']). ECs resisting denudation displayed a normal pattern of N-cadherin expression (Supplementary Data Fig. S5C').

DISCUSSION

We have demonstrated that VZ disruption occurs consistently in infants with IVH. The timetable of normal neurogenesis, ependymogenesis, and astrogliogenesis in the developing human brain ([Fig. 7J]) provides the basis to suggest strongly that developmental sequelae depend on the timing of IVH and the extension of the VZ disruption ([61–6]). Seven cell types, which correspond to the differentiation of NSCs (our types 1–3) into multiciliated ependyma (type 4–7), were identified in the VZ IVH cases, and considerable amounts of normal VZ but multiple sites of altered VZ were prevalent. The disrupted regions were characterized by loss (denudation) of ciliated NSC and multiciliated ECs, absence of normal radial processes, eruption of cells into the ventricle, and PH and rosettes. GFAP-positive cells with cytological features of mature AS populated areas that could have been sites of VZ disruption. Regional differences occurred in both control and IVH cases such that the MW of the LV appeared to differentiate into multiciliated ependyma earlier than the lateral and DWs.

FIGURE 4. Continued
re-populated by AS and 1 disruption site through which NPCs reach the ventricle (broken arrow). **(B')** The same picture as in panel **(B)** using only the channel for GFAP to highlight the cytological features that identify the GFAP-positive cells as AS, i.e. short thick nonradial processes. The nondisrupted VZ is formed by normal GFAP-positive NSCs with long thin radial processes. **(C, C')** Detailed magnification of the disrupted area shown in panel **(B)**. The arrow points to the border between the disrupted and nondisrupted VZ. The abundance of βIII-tubulin-positive NPCs masks the radial processes of NSCs seen in **C'**. AS fill the disrupted area (asterisk). **(D)** At very high magnification the normal appearance of AQP4-positive NSCs with cascades of βIII-tubulin-positive NPCs between the stem cell processes can be seen in a region of nondisrupted VZ. **(E)** Area similar to that shown in panel **(C)**; AS filling the disrupted VZ express AQP4. The arrow points to the border between the disrupted and nondisrupted VZ. **(F, G)** PH (arrows) from the region demarcated in Figure 3B. Note that cells contained within the PHs are all βIII-tubulin-positive. Scale bars: **A, B, B'**, 100 μm; **C, C'**, 25 μm; **D, E**, 10 μm; **F, G**, 100 μm.
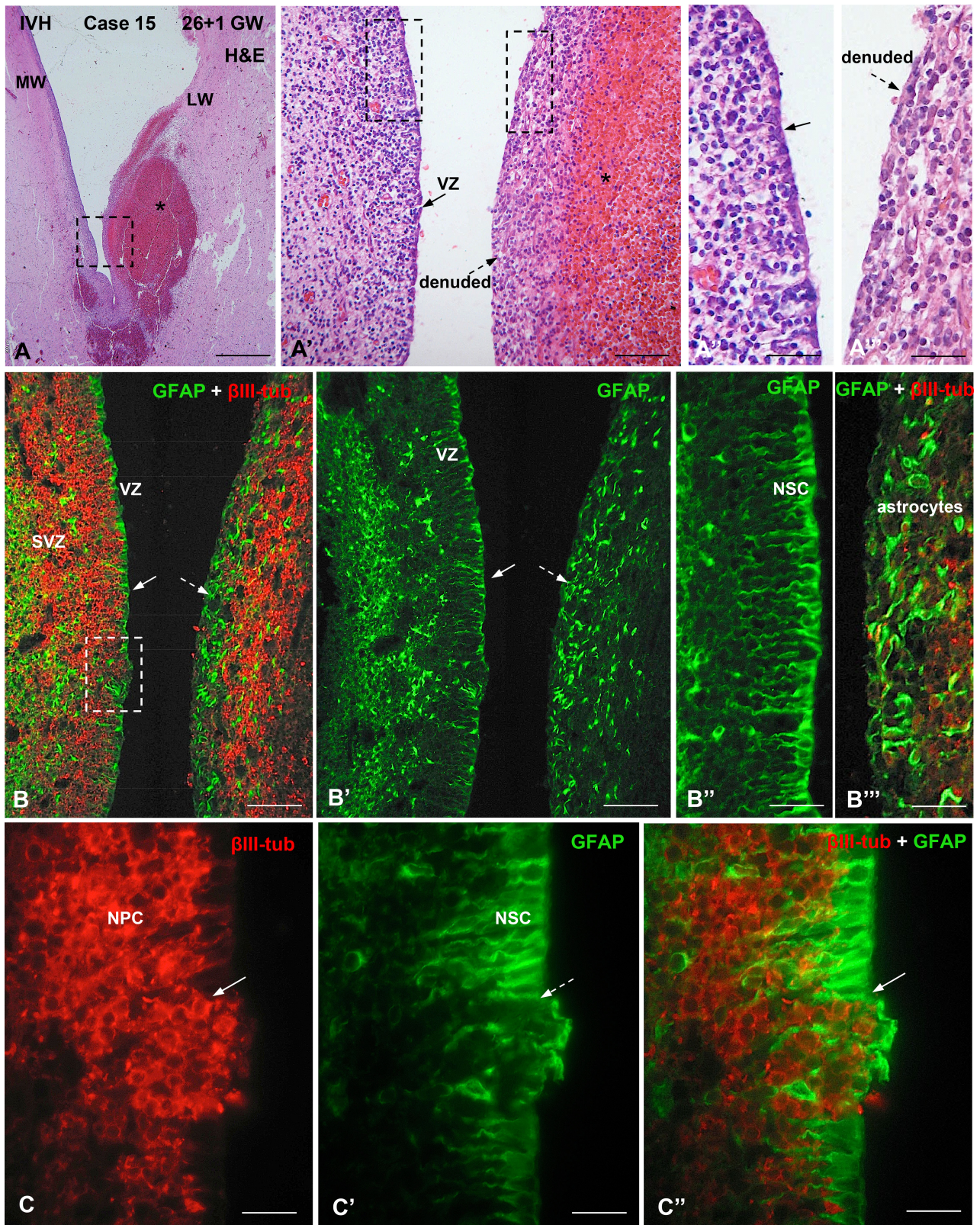
FIGURE 5. Photomicrographs from Case 15 of a preterm infant at 27 weeks of gestation with IVH-3 or 4 and large subependymal hemorrhages. **(A-A''')**. A H&E-stained section through the LW and MW of a LV showing several hemorrhages in the subependymal region (asterisk). The area framed in **(A)** is shown in **(A')**. **(A')** The LW (left) of a LV displays a normal cellular

These findings help characterize neuroepithelial evolution of the early normal preterm human brain as well as expand interpretations of the neuropathology that accompanies IVH.

Limitations

This study is limited by the relatively small number of cases due to our strict selection of cases of infants diagnosed with IVH. In particular, the lack of age-matched control specimens for the 2 older age groups opens the possibility that other causes may contribute to VZ disruption, such as systemic inflammation or acute events like cardiac arrest. Our samples included only the frontal horn of the LV, and other parts of the ventricular system may or may not have exhibited hemorrhage and/or VZ disruption. Fixation and processing of the samples is also a limitation because formaldehyde and Bouin's fixative may have effects on the accessibility of antibodies to their epitopes, which could produce immunostaining variations in cell bodies and cilia. Clinically, the actual time of the hemorrhagic episode is always difficult to establish; thus, we estimated the approximate time interval between IVH and death in these cases by considering the dates of birth, US diagnosis of IVH, and death. Our ongoing studies should help fill in all of these gaps.

Regional Variations in the Walls of the LVs

Our results indicate that in human preterm infants there are early differences between the medial and the LWs–DWs of the LVs. These differences are similar to those seen in the developing rat brain where during the last few days of fetal life the medial ventricular wall is already lined by multiciliated ependyma while the LWs and DWs contain NSCs (18). In mice, this heterogeneity persists well into adulthood (67). Our observations corroborate those of Sarnat (55, 56) and indicate that mature ECs are present in the MW by 23 GW and appear later in the LWs and DWs. This may suggest that in early stages of VZ development, the MW is primarily involved in CSF hydrodynamics (61–4, 68–70) and guiding neuronal migration (65), while the LW–DWs still possess a neurogenetic function. The fact that in more mature fetuses the denuded ventricular areas are much larger indicates that several disruption foci grow to form extended denuded areas.

Evolving Cell Types of the VZ: Evidence for an Ependymogenesis Program

According to Rakic, the proliferative zone of the human telencephalon contains complex progenitor cell groups that change phenotype during the course of development (66). In very young embryos (5–6 GW), the VZ contains a mixed population of cells; most of them express only stem cell markers such as GFAP and glutamate astrocyte transporter (71), while others also express neuronal markers (βIII-tubulin, microtubule-associated protein-2) indicating their pluripotent capacity (72). Later in development (10–22 GW), vimentin-positive and GFAP-positive cells displaying a long basal process persist. Proliferation of GFAP-positive cells of the VZ occurs until 23 GW, coinciding with the formation of the ependyma (72). According to Gould et al (73), in early pregnancy the VZ is formed by GFAP-positive NSCs, whereas in late pregnancy the VZ is formed by GFAP-positive ECs with short basal processes. Sarnat (55–7) has also followed in human fetuses the temporal and spatial differentiation of cells lining the fetal ventricular system. In these studies, he has regarded all cells lining the fetal ventricular system as ependymal. Using this criterion, he concluded that the expression of GFAP and vimentin in fetal ECs follows a precise regional and temporal distribution (55, 56). Sarnat (57) also made no distinction between NSCs, differentiating ECs and mature multiciliated ependyma. He found that GFAP was co-expressed with vimentin in most fetal ECs, but at birth only scattered ECs still expressed GFAP and it disappeared entirely within the first few weeks of postnatal life. The disappearance of GFAP in ECs has been challenged recently by Haemmerle et al (67), who report that GFAP-positive AS with a single cilium comprise up to 37% of the ependymal lining in adult rats; these cells, termed B1 cells, are not considered to be radial glia but they appear to be responsible for producing NSCs in adults.

In spite of these reports, the true process of ependymogenesis in the human remains largely unknown, primarily because of limitations in obtaining samples of the ventricular walls from selected regions and specific gestational ages. Our classification of 7 cell types within the VZ, based on immunoreactivity to GFAP, AQP4, βIV-, and βIII-tubulin, as well as the appearance of a basal (radial) process and single or multiple cilia, was designed to help clarify the differentiation of ECs. In general, our Type 1, 2 and 3 cells (which exhibit a long basal process, a single cilium, and expression of GFAP throughout the cytoplasm and AQP4 in the plasma membrane)

FIGURE 5. Continued
arrangement of the ventricular (VZ) and SVZs while the MW (right), bearing a large hemorrhage (asterisk), is denuded. The areas framed are shown in **A''** and **A'''**. (**A''**, **A'''**) LW (**A''**) and MW (**A'''**); the former displays a normal VZ (solid arrow) while the latter is denuded. (**B**) Section adjacent to that of panel **A**; double immunofluorescence for GFAP (green) and βIII-tubulin (red). The LW (left) is lined by GFAP-positive cells (VZ, solid arrow) and the SVZ contains βIII-tubulin-positive cells. The denuded MW contains a thick layer of GFAP-positive AS (dashed arrow) and numerous, somewhat disorganized βIII-tubulin-positive cells. (**B'**) Same field as in **B** using only the channel for GFAP. Solid and dashed arrows indicate the areas shown in **B''** and **B'''**, respectively. (**B''**, **B'''**) The LW (**B''**) is lined by a layer of NSCs while the denuded MW (**B'''**) is formed by AS. (**C–C''**) Detailed magnification of the area framed in **B**, showing a small area of VZ disruption in the LW (arrow). The disrupted area is occupied by NPCs and GFAP-positive AS. The NSCs of the VZ are GFAP-positive. Scale bars: **A**, 300 μm; **A'**, 100 μm; **A''A'''**, 50 μm; **B, B'**, 10 μm; **B''**, **B'''**, 50 μm; **C–C''**, 25 μm.
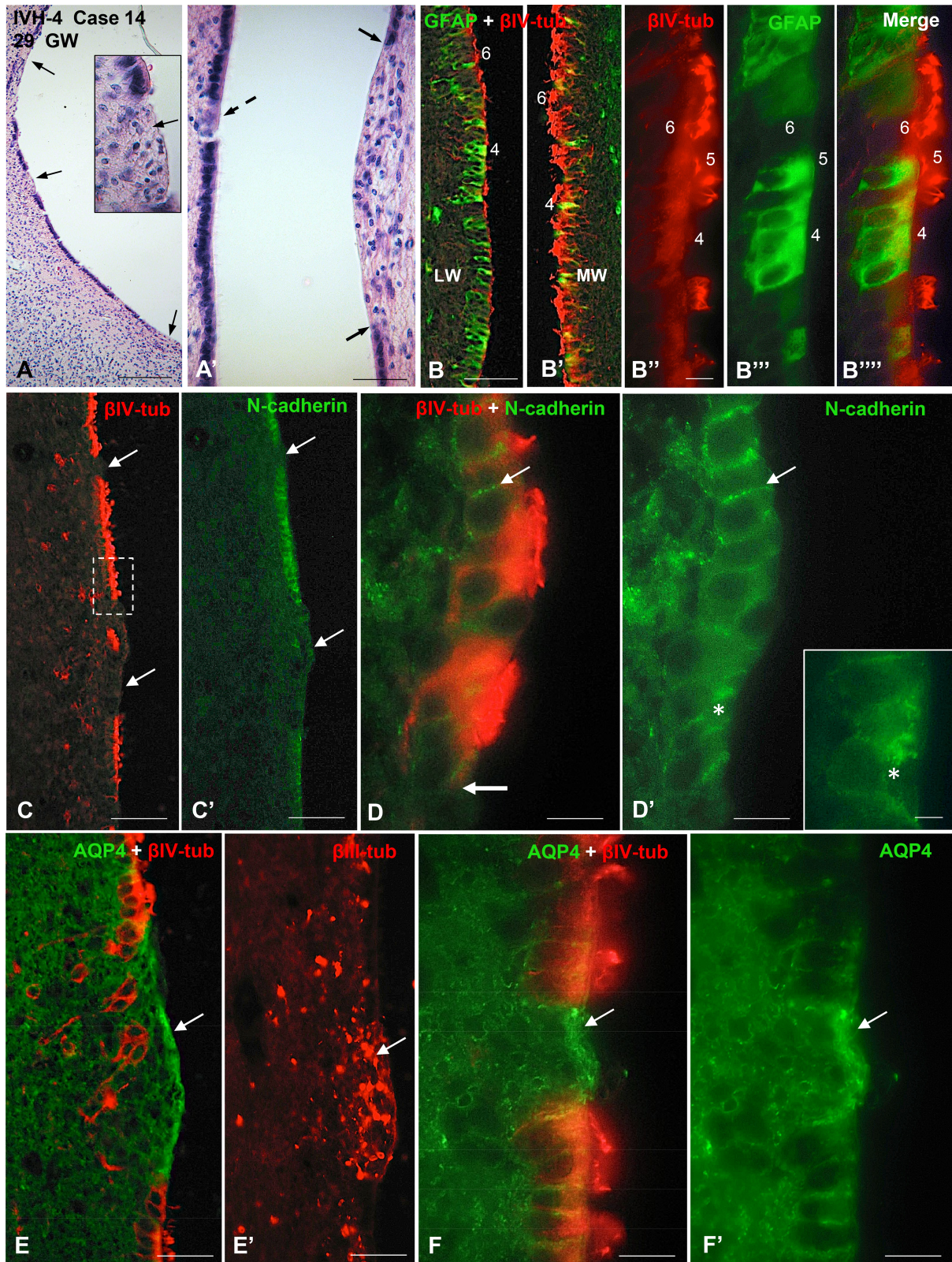
FIGURE 6. Photomicrographs from Case 14 of a preterm infant with IVH-4 who died at 29 GW. The neuropathological analysis revealed subependymal hemorrhage in the left hemisphere and a massive IVH. **(A)** Wall of a LV showing several areas of VZ disruption (arrows). Inset: magnification of a disruption focus shown in a (middle arrow). The area with ependymal denudation

seem to correspond to early-forming, noncommitted proliferating NSCs or radial glia described by others (52–4, 56, 57, 60). In our specimens, these cells were the main cell type in the VZ of the youngest fetuses studied. We suggest that our cell types 4–6 reflect progressive stages of EC maturation, based primarily on an absent or shortened basal process, the co-expression of βIV-tubulin and GFAP, the expression of βIV-tubulin but not GFAP, and the presence of multiple cilia. These cells may evolve into the mature multiciliated, βIV-tubulin-positive, ECs present during the last trimester of fetal life; with persistent expression of GFAP and elaboration of a single cilium, some of these cells may correspond to the B1 AS thought to produce NPs in adulthood (67). Further studies are required to determine if the different VZ cell types differentiate from a common epithelial cell precursor and how their phenotype is linked genetically to specific signaling pathways.

Novel Contributors to the Pathogenesis of IVH and PHH

Although the pathogenesis of IVH is usually attributed to the intrinsic fragility of the germinal matrix vasculature and impairments of CSF flow and absorption as part of the processes leading to hydrocephalus (4, 74), there may be other mechanisms that contribute to the development of hydrocephalus. Studies on hyh mice (which develop congenital perinatal aqueduct stenosis) have supported the concept of genetic defects in the cell junction complexes that alter the VZ, resulting in the disassembling and loss of the VZ cells (20, 24–6, 37–41). This phenomenon was first described as ependymal denudation (39) and later designated as VZ disruption (18, 21, 22, 36). The process of VZ disruption has been found in a series of mutant rodents with hereditary hydrocephalus (75–79), in other human cases with fetal onset hydrocephalus (22, 27, 31, 32), and following intraventricular injections of a thrombin by-product in fetal mice (80). A good body of evidence indicates that disruption of the VZ arises from a pathway involving alterations of vesicle trafficking, abnormal cell junctions and loss of VZ integrity (81). In brief, areas of the VZ about to become denuded display disorganized VZ/ECs with an abnormal subcellular location of N-cadherin and connexin 43 (18, 21, 23, 32). The abnormal subcellular location of N-cadherin in VZ cells close to undergoing disruption suggests that in IVH cases, as in fetal-onset hydrocephalus (18, 21, 27, 32, 45), a junction pathology of NSCs and ECs occurs at rather early phases of brain development and may be accentuated by hemorrhage.

PH are arrested neuroblasts whose migration has been halted (18, 23, 81). In humans, the formation of heteropia occurs between 12 and 22 GW (82, 83). Based on this timing, our observation of heterotopia raises the possibility that processes other than IVH may contribute to these migrational abnormalities or, possibly, VZ itself. Additional studies are required to delineate the relationship and timing of IVH to VZ disruption and its developmental sequelae.

It is possible that specific alterations in the formation of both primary and motile cilia could contribute to VZ disruption, and many congenital ciliopathy models develop ventriculomegaly (33, 64, 84). In a strain of mice with ciliopathy and hydrocephalus, expression of the forkhead transcription factor FoxJ1 is required for normal differentiation of ECs as well as some AS that function as postnatal NSCs (85). Likewise, Tissir et al found that impaired development and planar organization of the cell polarity cadherins Celsr2 and Celsr3, which control ciliary beating, leads to abnormal CSF dynamics and hydrocephalus (86). While the role that cilia and cell polarity may play in VZ disruption has yet to be defined, the fact that in our specimens the alterations were intermittent and mixed with normal VZ/SVZ regions implies that genetic targeting may be quite precise.

Potential Effects of VZ Disruption on CSF Physiology and Neurodevelopment

Ciliary beating of ECs may be responsible, at least in part, for the laminar flow of CSF occurring on the ventricular surface (61, 68, 70, 87, 88). This is strongly supported by the fact that primary ciliary dyskinesia leads to the development of hydrocephalus (70, 89–91). Long ago, Worthington and Cathcart (89, 92) concluded that small areas of ependymal injury and ciliary destruction may affect CSF flow far beyond the region of local damage in humans. We have seen that during the third trimester of gestation VZ disruption leaves large areas of the ventricular walls denuded. It seems likely that these local disturbances may impair CSF flow and contribute to the progressive development of hydrocephalus in IVH.

FIGURE 6. Continued

(arrow) is occupied by small basophilic cells. H&E staining. **(A′)** Opposite walls of a LV showing a small (dashed arrow) and a large (between 2 arrowheads) areas of VZ disruption. **(B, B′)** Section through a nonaffected region of a LV. Double immunofluorescence for GFAP (green) and βIV-tubulin (red). The VZ of the LW is formed by a mixed population of GFAP-positive cells (type 4) and βIV-tubulin-positive multiciliated cells (type 6) while that of the MW is mostly lined by type 6 cells. **(B″–B″″)** Detailed magnification of **(B)**; the VZ of the LW is formed by GFAP-positive cells with no cilia (type 4), GFAP-positive cells with cilia (type 5) and βIV-tubulin-positive multiciliated cells (type 6). **(C–F)** Sections adjacent to that shown in panel A processed for double immunofluorescence for βIV-tubulin (red) and N-cadherin (green), AQP4 (green) and βIV-tubulin (red) and for βIII-tubulin (red), as indicated. **(C, C′)** Areas of ependymal denudation and lacking N-cadherin expression are shown (arrows). The area framed is shown in **(D)**. **(D, D′)** ECs in the nondisrupted regions express N-cadherin at the lateral plasma membrane domain (thin arrow) while those at the disruption front (thick arrow) contain N-cadherin as cytoplasmic masses (asterisk). Inset. Detailed magnification of **D′**. **(E)** An area of ependymal denudation is lined by AQP4-positive AS (arrow). **(E′)** Section adjacent to that of **E** showing βIII-tubulin NPCs clustered at the disrupted area (arrow). **(F, F′)** A small area of ependymal disruption is occupied by AQP4-positive AS (arrow). Scale bars: **A**, 250 μm; **A′–B′, C, C′**, 100 μm; **B″**, 20 μm; **D, D′**, 10 μm; **D′** insert, 4 μm; **E, E′**, 50 μm; **F, F′**, 10 μm.
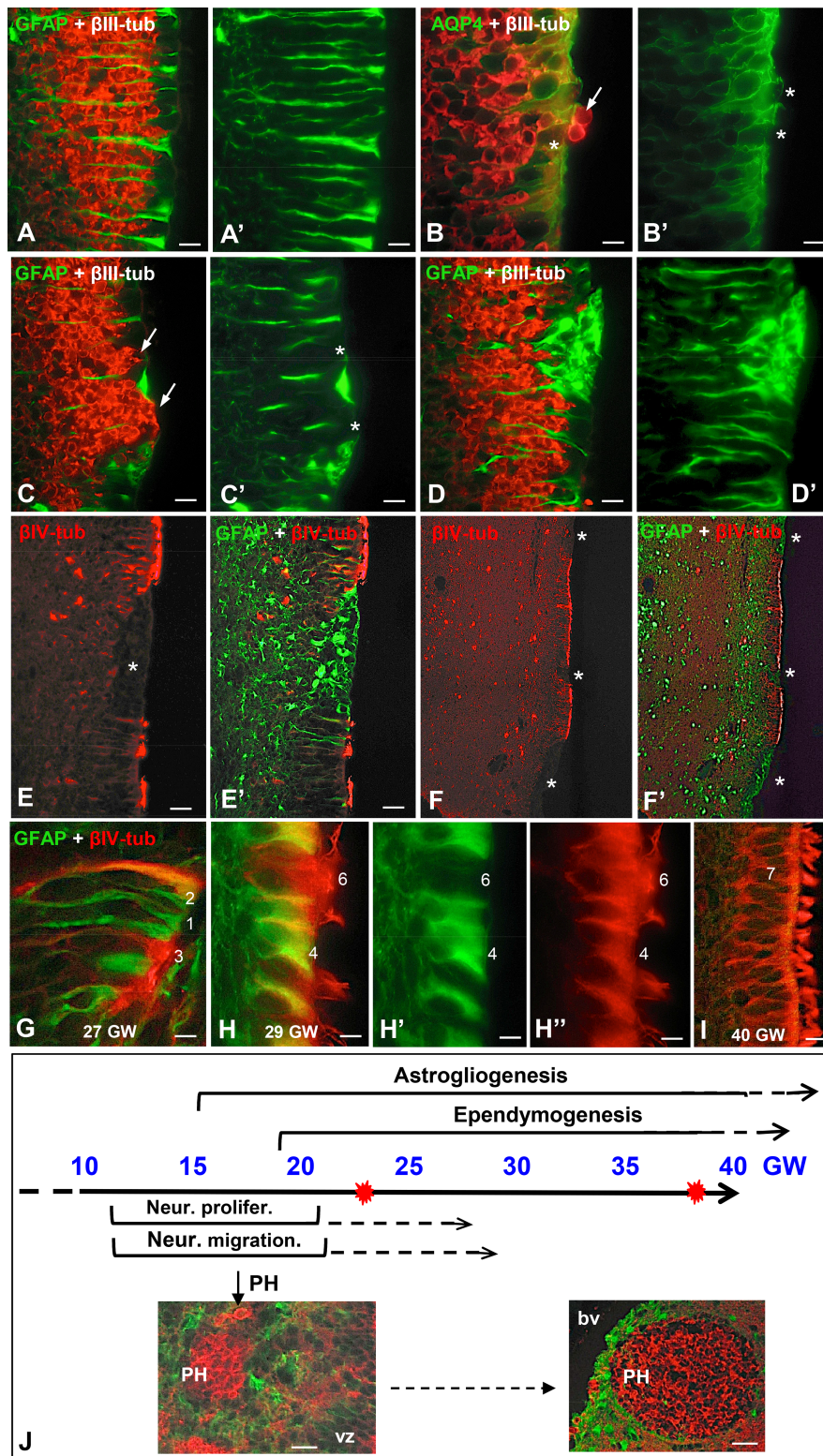
FIGURE 7. Panel summarizing the proposed sequence of events of the disruption process affecting the VZ and SVZs of preterm neonates with IVH. **(A–F)** At early gestational ages, the nonaffected regions of the VZ are formed by a contiguous layer of NSCs and the SVZ contains clustered NPC aligned along the radial processes of the NSC **(A, A')**. Initially, the disruption involves a few NSC allowing a few NPC to reach the ventricle **(B, B',** arrow, asterisks). Then the disruption focus grows leaving an area devoid of NSC **(C',** asterisks) occupied by clusters of NPC that become exposed to the CSF **(C,** arrows). At a later phase, the area devoid of NSC is occupied by AS (asterisk) that fill the gap and prevent NPC from reaching the ventricle **(D, D')**. At more advanced

FIGURE 7. Continued

gestational ages, the VZ formed by multiciliated cells also undergoes disruption (**E,** asterisk) and these foci are also sealed by a layer of AS (**E',** asterisk). The different extents of the disruption foci co-existing in the same case, their "repair" by a patch of AS (**F, F'**), and the existence of PH suggest that the disruption process starts early in development and continues along a lengthy period of fetal life. (**G–I**) Different cell types are present in the VZ. The numbers indicate the probable differentiation stages from NSC (no. 1) to multiciliated ependyma (no. 7). Type 5 cell is not shown; see Figure 6B''. (**J**) Panel summarizing the timetable of key events in the developing human brain. The bulk of neural proliferation and neural migration occurs between 12 and 22 GW; then both processes decrease progressively. The process of ependymogenesis starts at about 18 GW and is completed after birth. Gliogenesis starts at about 15 GW and continues for several months after birth. PH are formed during the period of neuroblast migration and then become structured, progressively moving away from the ventricle as the brain grows. VZ, ventricular zone; bp, lumen of blood vessel; red stars, age of the youngest and oldest IVH cases. Scale bars: **A, A'**, 25 μm; **B, B'**, 12 μm; **C–E**, 50 μm; **F, F'**, 125 μm; **F, F'**, J inserts, 50 μm.

Nevertheless, we cannot rule out the possibility that other traditional mechanisms, such as increased CSF pulsatility (93), CSF bulk flow obstruction and absorption, or mass effects of the hemorrhage, are primarily responsible for the ventriculomegaly we have observed.

Loss of radial glia and ECs into the CSF and the formation of heterotopia may also have profound neurodevelopmental consequences. Our findings of cells in the ventricles confirm previous observations in rodents and humans (18, 20–2, 32) and are supported by Krueger et al (46) who reported the presence of NSC and progenitor cells in the CSF of preterm infants with PHH. Malik et al (94) showed that neurogenesis in the ventricular and SVZs of the human cerebral cortex continues into the third trimester, and that premature birth diminishes this "late" neurogenesis. It is reasonable to assume that IVH during this vulnerable period may have grave consequences yet the full impact of IVH, even that of lower-grades, on neurodevelopment is little known (95). Taking into account the aforementioned regional variations in the walls of the LVs, the repercussions of the disruption of the VZ could probably be different in less mature areas (DW–LW), which are mainly composed by RG cells and where neurogenesis impairment is found (heterotopy and neural migration), as opposed to within the mature areas (MW) where the VZ is mainly formed by mature ECs (55, 56). Proliferation of cells in the germinal zone, the GE in particular, is suppressed within 24 hours after hemorrhage (96). The mechanism of such suppression is not clear, but the rapid effect suggests a direct cell-signaling pathway mediated by diffusible factors from the site of the hematoma. Decreased proliferation of germinal cells in the GE would affect production of GABAergic interneurons for the neocortex, while reduced oligodendrocyte development would have an adverse effect on cerebral myelination (96).

Possible Repair Mechanisms in IVH

Sarnat (97) presents an interesting view about how AS may respond to ependymal injury, especially during the stretching and tearing that occurs with ventriculomegaly. He concluded that after injury the ependyma "does not regenerate at any age". Our observations are consistent with his observations on cytopathology, particularly his description of discontinuities that become filled with processes of subventricular AS. In hyh mice with congenital hydrocephalus, the missing VZ appears to be replaced by a layer of AS forming a new interface between the CSF and the brain parenchyma (25, 40). This phenomenon has also been described in human fetuses with hydrocephalus (27, 32, 97). In hyh mice, the new surface layer of AS shares some phenotypic and functional features with the lost ependyma suggesting that in fetal-onset hydrocephalus the astrocyte assembly at the denuded ventricular walls may function as a CSF–brain barrier (20). Indirect evidence for local differentiation of these new AS has been provided in the present investigation. It seems reasonable to postulate that in preterm IVH infants the astrocyte patch may prevent NSCs and ECs from falling into the ventricle and reestablish some of the functions of the lost ependyma. Further long-term studies are needed to determine if the GFAP-positive and AQP4-positive cells that we see lining the ventricles are capable of establishing cell-to-cell contacts and acquiring some of the properties of the lost VZ.

REFERENCES

1. McCrea HJ, Ment LR. The diagnosis, management, and postnatal prevention of intraventricular hemorrhage in the preterm neonate. Clin Perinatol 2008;35:777–92
2. Adams-Chapman I, Hansen NI, Stoll BJ, et al. Neurodevelopmental outcome of extremely low birth weight infants with posthemorrhagic hydrocephalus requiring shunt insertion. Pediatrics 2008;121:e1167–77
3. Stoll BJ, Hansen NI, Bell EF, et al. Trends in care practices, morbidity, and mortality of extremely preterm neonates, 1993-2012. Jama 2015; 314:1039–51
4. Robinson S. Neonatal posthemorrhagic hydrocephalus from prematurity: pathophysiology and current treatment concepts. J Neurosurg Pediatr 2012;9:242–58
5. Dykes FD, Dunbar B, Lazarra A, et al. Posthemorrhagic hydrocephalus in high-risk preterm infants: natural history, management, and long-term outcome. J Pediat 1989;114:611–8
6. Limbrick DD, Jr, Mathur A, Johnston JM, et al. Neurosurgical treatment of progressive posthemorrhagic ventricular dilation in preterm infants: a 10-year single-institution study. J Neurosurg Pediatr 2010;6:224–30
7. Murphy BP, Inder TE, Rooks V, et al. Posthaemorrhagic ventricular dilatation in the premature infant: natural history and predictors of outcome. Arch Dis Child Fetal Neonatal Ed 2002;87:F37–41
8. Vassilyadi M, Tataryn Z, Shamji MF, et al. Functional outcomes among premature infants with intraventricular hemorrhage. Pediatr Neurosurg 2009;45:247–55
9. Bhattathiri PS, Gregson B, Prasad KS, et al. Intraventricular hemorrhage and hydrocephalus after spontaneous intracerebral hemorrhage: results from the STICH trial. Acta Neurochir Suppl 2006;96:65–8
10. Radic JA, Vincer M, McNeely PD. Temporal trends of intraventricular hemorrhage of prematurity in Nova Scotia from 1993 to 2012. J Neurosurg Pediatr 2015;15:573–9

11. Christian EA, Jin DL, Attenello F, et al. Trends in hospitalization of pre-term infants with intraventricular hemorrhage and hydrocephalus in the United States, 2000-2010. J Neurosurg Pediatr 2017;260–269

12. Tsitouras V, Sgouros S. Infantile posthemorrhagic hydrocephalus. Childs Nerv Syst 2011;27:1595–608

13. Fletcher JM, Landry SH, Bohan TP, et al. Effects of intraventricular hemorrhage and hydrocephalus on the long-term neurobehavioral development of preterm very-low-birthweight infants. Dev Med Child Neurol 1997;39:596–606

14. Garton T, Keep RF, Wilkinson DA, et al. Intraventricular hemorrhage: the role of blood components in secondary injury and hydrocephalus. Trans Stroke Res 2016;7:447–51

15. Strahle J, Garton H, Maher C, et al. Mechanisms of hydrocephalus after neonatal and adult intraventricular hemorrhage. Trans Stroke Res 2012; 1–14

16. Larroche JC. Post-haemorrhagic hydrocephalus in infancy. Anatomical study. Biol Neonate 1972;20:287–99

17. Boop FA, Posthemorrhagic hydrocephalus of prematurity.In: Cinalli G, ed. Pediatric Hydrocephalus. Italy: Springer-Verlag 2005:121–31

18. Guerra M, Henzi R, Ortloff A, et al. A cell junction pathology of neural stem cells is associated with ventricular zone disruption, hydrocephalus and abnormal neurogenesis. J Neuropathol Exp Neurol 2015;74:653–71

19. Ortloff AR, Vio K, Guerra M, et al. Role of the subcommissural organ in the pathogenesis of congenital hydrocephalus in the HTx rat. Cell Tiss Res 2013;352:707–25

20. Roales-Bujan R, Paez P, Guerra M, et al. Astrocytes acquire morphological and functional characteristics of ependymal cells following disruption of ependyma in hydrocephalus. Acta Neuropathol 2012;124: 531–46

21. Rodriguez EM, Guerra MM, Vio K, et al. A cell junction pathology of neural stem cells leads to abnormal neurogenesis and hydrocephalus. Biol Res 2012;45:231–42

22. Guerra M, Sival D, Jimenez A, et al. Defects in cell-cell junctions lead to neuroepithelial/ependymal denudation in the telencephalon of human hydrocephalic foetuses. Cerebrospinal Fluid Res 2010;7:S56

23. Ferland RJ, Batiz LF, Neal J, et al. Disruption of neural progenitors along the ventricular and subventricular zones in periventricular heterotopia. Hum Mol Genet 2009;18:497–516

24. Jimenez AJ, Garcia-Verdugo JM, Gonzalez CA, et al. Disruption of the neurogenic niche in the subventricular zone of postnatal hydrocephalic hyh mice. J Neuropathol Exp Neurol 2009;68:1006–20

25. Paez P, Batiz LF, Roales-Bujan R, et al. Patterned neuropathologic events occurring in hyh congenital hydrocephalic mutant mice. J Neuropathol Exp Neurol 2007;66:1082–92

26. Batiz F, Paez P, Jimenez AJ, et al. Clinical and neuropathological evolution of the hydrocephalus developed by the mutant mouse hyh. Cerebrospinal Fluid Res 2005;2:S9

27. Dominguez-Pinos MD, Paez P, Jimenez AJ, et al. Ependymal denudation and alterations of the subventricular zone occur in human fetuses with a moderate communicating hydrocephalus. J Neuropathol Exp Neurol 2005;64:595–604

28. Acabchuk RL, Sun Y, Wolferz R, Jr, et al. 3D Modeling of the lateral ventricles and histological characterization of periventricular tissue in humans and mouse. JoVE 2015;e52328.

29. Shook BA, Lennington JB, Acabchuk RL, et al. Ventriculomegaly associated with ependymal gliosis and declines in barrier integrity in the aging human and mouse brain. Aging Cell 2014;13:3340–50

30. Halling M, An Analysis of the Association Between Ependymal Integrity and Ventriculomegaly. Anatomy and neurobiology, Vol. Masters. Storrs, CT: University of Connecticut 2013

31. Ortega E, Munoz RI, Luza N, et al. The value of early and comprehensive diagnoses in a human fetus with hydrocephalus and progressive obliteration of the aqueduct of Sylvius: case report. BMC Neurol 2016;16:45

32. Sival DA, Guerra M, den Dunnen WF, et al. Neuroependymal denudation is in progress in full-term human foetal spina bifida aperta. Brain Pathol 2011;21:163–79

33. Vogel TW, Carter CS, Abode-Iyamah K, et al. The role of primary cilia in the pathophysiology of neural tube defects. (Review). Neurosurg Focus 2012;33:E2

34. Sarkisian MR, Guadiana SM. Influences of primary cilia on cortical morphogenesis and neuronal subtype maturation. Neuroscientist 2015; 21: 136–51

35. Norris DP, Grimes DT. Mouse models of ciliopathies: the state of the art. Dis Mod Mech 2012;5:299–312

36. Sotak BN, Gleeson JG. Can't get there from here: cilia and hydrocephalus. Nat Med 2012;18:1742–3

37. Batiz LF, Paez P, Jimenez AJ, et al. Heterogeneous expression of hydrocephalic phenotype in the hyh mice carrying a point mutation in [alpha]-SNAP. Neurobiol Dis 2006;23:152–68

38. Perez-Figares JM, Jimenez AJ, Perez-Martin M, et al. Spontaneous congenital hydrocephalus in the mutant mouse hyh. Changes in the ventricular system and the subcommissural organ. J Neuropathol Exp Neurol 1998;57:188–202

39. Jimenez AJ, Tome M, Paez P, et al. A programmed ependymal denudation precedes congenital hydrocephalus in the hyh mutant mouse. J Neuropathol Exp Neurol 2001;60:1105–19

40. Wagner C, Batiz LF, Rodriguez S, et al. Cellular mechanisms involved in the stenosis and obliteration of the cerebral aqueduct of hyh mutant mice developing congenital hydrocephalus. J Neuropathol Exp Neurol 2003;62:1019–40

41. Batiz LF, Jimenez AJ, Guerra M, et al. New ependymal cells are born postnatally in two discrete regions of the mouse brain and support ventricular enlargement in hydrocephalus. Acta Neuropathol 2011;121: 721–35

42. Bystron I, Blakemore C, Rakic P. Development of the human cerebral cortex: Boulder Committee revisited. Nat Rev Neurosci 2008;9:110–22

43. Morales DM, Townsend RR, Malone JP, et al. Alterations in protein regulators of neurodevelopment in the cerebrospinal fluid of infants with posthemorrhagic hydrocephalus of prematurity. Mol Cell Proteomics 2012;11:M111 011973

44. Morales DM, Silver SA, Morgan CD, et al. Lumbar cerebrospinal fluid biomarkers of post-hemorrhagic hydrocephalus of prematurity - amyloid precursor protein, soluble APPα, and L1 cell adhesion molecule. Neurosurg 2017; 80:82–90.

45. Jimenez AJ, Dominguez-Pinos MD, Gomez-Rolden MD, et al. Common neuropathological events are present in different forms of human foetal-neonatal onset congenital hydrocephalus. In 57th Annual Meeting of the Society for Research in Hydrocephalus and Spina Bifida. Cologne, Germany 2013

46. Krueger RC, Jr., Wu H, Zandian M, et al. Neural progenitors populate the cerebrospinal fluid of preterm patients with hydrocephalus. J Pediatr 2006;148:337–40

47. Fukumizu M, Takashima S, Becker LE. Glial reaction in periventricular areas of the brainstem in fetal and neonatal posthemorrhagic hydrocephalus and congenital hydrocephalus. Brain Devel 1996;18:40–5

48. Takashima S, Fukumizu M. Pathology of congenital aqueductal stenosis and posthemorrhagic hydrocephalus. No to Hattatsu 1994;26:216–21

49. Papile LA, Burstein J, Burstein R, et al. Incidence and evolution of subependymal and intraventricular hemorrhage: a study of infants with birth weights less than 1,500 gm. J Pediatr 1978;92:529–34

50. Volpe JJ. Intraventricular hemorrhage and brain injury in the premature infant. Neuropathology and pathogenesis. Clin Perinatol 1989;16:361–86

51. O'Hayon BB, Drake JM, Ossip MG, et al. Frontal and occipital horn ratio: A linear estimate of ventricular size for multiple imaging modalities in pediatric hydrocephalus. Pediatr Neurosurg 1998;29:245–9

52. De Juan Romero C, Borrell V. Coevolution of radial glial cells and the cerebral cortex. Glia 2015;63:1303–19

53. Kriegstein A, Alvarez-Buylla A. The glial nature of embryonic and adult neural stem cells. Annu Rev Neurosci 2009;32:149–84

54. Bayatti N, Moss JA, Sun L, et al. A molecular neuroanatomical study of the developing human neocortex from 8 to 17 postconceptional weeks revealing the early differentiation of the subplate and subventricular zone. Cereb Cortex 2008;18:1536–48

55. Sarnat HB. Role of human fetal ependyma. Pediatr Neurol 1992;8: 163–78

56. Sarnat HB. Regional differentiation of the human fetal ependyma: immunocytochemical markers. J Neuropathol Exp Neurol 1992;51:58–75

57. Sarnat HB. Histochemistry and immunocytochemistry of the developing ependyma and choroid plexus. Microsc Res Tech 1998;41:14–28

58. Afsharkhas L, Khalessi N, Karimi Panah M. Intraventricular hemorrhage in term neonates: sources, severity and outcome. Iran J Child Neurol 2015;9:34–9

59. Gardner SL, Carter BS, Enzman-Hines M, et al. Merenstein and Gardner Handbook of Neonatal Intensive Care, 7th edn. Saint Louis, MO, USA: Mosby Elsevier 2011

60. Javaherian A, Kriegstein A. A stem cell niche for intermediate progenitor cells of the embryonic cortex. Cereb Cortex 2009;19(Suppl 1):i70–7

61. Swiderski RE, Agassandian K, Ross JL, et al. Structural defects in cilia of the choroid plexus, subfornical organ and ventricular ependyma are associated with ventriculomegaly. Fluids Barriers CNS 2012;9:22

62. Breunig JJ, Arellano JI, Rakic P. Cilia in the brain: going with the flow. Nat Neurosci 2010;13:654–5

63. Merchant M, Evangelista M, Luoh SM, et al. Loss of the serine/threonine kinase fused results in postnatal growth defects and lethality due to progressive hydrocephalus. Mol Cell Biol 2005;25:7054–68

64. Banizs B, Pike MM, Millican CL, et al. Dysfunctional cilia lead to altered ependyma and choroid plexus function, and result in the formation of hydrocephalus. Development 2005;132:5329–39

65. Sawamoto K, Wichterle H, Gonzalez-Perez O, et al. New neurons follow the flow of cerebrospinal fluid in the adult brain. Science 2006;311:629–32

66. Rakic P. Elusive radial glial cells: historical and evolutionary perspective. Glia 2003;43:19–32

67. Haemmerle CA, Nogueira MI, Watanabe IS. The neural elements in the lining of the ventricular-subventricular zone: making an old story new by high-resolution scanning electron microscopy. Front Neuroanat 2015;9:134

68. Milhorat TH. The third circulation revisited. J Neurosurg 1975;42:628–45

69. Ohata S, Nakatani J, Herranz-Perez V, et al. Loss of dishevelleds disrupts planar polarity in ependymal motile cilia and results in hydrocephalus. Neuron 2014;83:558–71

70. Appelbe OK, Bollman B, Attarwala A, et al. Disruption of the mouse *Jhy* gene causes abnormal ciliary microtubule patterning and juvenile hydrocephalus. Dev Biol 2013;382:172–85.

71. Chandrasekaran A, Avci HX, Leist M, et al. Astrocyte differentiation of human pluripotent stem cells: new tools for neurological disorder research. Front Cell Neurosci 2016;10:

72. Zecevic N. Specific characteristic of radial glia in the human fetal telencephalon. Glia 2004;48:27–35

73. Gould SJ, Howard S, Papadaki L. The development of ependyma in the human fetal brain: an immunohistological and electron microscopic study. Dev Brain Res 1990;55:255–67

74. Ballabh P. Intraventricular hemorrhage in premature infants - mechanism of disease. Pediat Res 2010;67:1–8

75. Klezovitch O, Fernandez TE, Tapscott SJ, et al. Loss of cell polarity causes severe brain dysplasia in Lgl1 knockout mice. Genes Dev 2004;18:559–71

76. Nechiporuk T, Fernandez TE, Vasioukhin V. Failure of epithelial tube maintenance causes hydrocephalus and renal cysts in Dlg5-/- mice. Dev Cell 2007;13:338–50

77. Ma X, Bao J, Adelstein RS. Loss of cell adhesion causes hydrocephalus in nonmuscle myosin II-B-ablated and mutated mice. Mol Biol Cell 2007;18:2305–12

78. Rasin MR, Gazula VR, Breunig JJ, et al. Numb and Numbl are required for maintenance of cadherin-based adhesion and polarity of neural progenitors. Nat Neurosci 2007;10:819–27

79. Imai F, Hirai S, Akimoto K, et al. Inactivation of aPKClambda results in the loss of adherens junctions in neuroepithelial cells without affecting neurogenesis in mouse neocortex. Development 2006;133:1735–44

80. Yung YC, Mutoh T, Lin ME, et al. Lysophosphatidic acid signaling may initiate fetal hydrocephalus. Sci Trans Med 2011;3:99ra87

81. Sheen VL. Periventricular heterotopia: shuttling of proteins through vesicles and actin in cortical development and disease. Scientifica (Cairo) 2012;2012:480129

82. Palmini A, Andermann F, de Grissac H, et al. Stages and patterns of centrifugal arrest of diffuse neuronal migration disorders. Dev Med Child Neurol 1993;35:331–9

83. Raymond AA, Fish DR, Stevens JM, et al. Subependymal heterotopia: a distinct neuronal migration disorder associated with epilepsy. J Neurol Neurosurg Psych 1994;57:1195–202

84. Laclef C. Primary cilia control different steps of brain development. Med Sci (Paris) 2014;30:980–90

85. Jacquet BV, Salinas-Mondragon R, Liang H, et al. FoxJ1-dependent gene expression is required for differentiation of radial glia into ependymal cells and a subset of astrocytes in the postnatal brain. Development 2009;136:4021–31

86. Tissir F, Qu Y, Montcouquiol M, et al. Lack of cadherins Celsr2 and Celsr3 impairs ependymal ciliogenesis, leading to fatal hydrocephalus. Nat Neurosci 2010;13:700–7

87. Cifuentes M, Rodriguez S, Perez J, et al. Decreased cerebrospinal fluid flow through the central canal of the spinal cord of rats immunologically deprived of Reissner's fibre. Exp Brain Res 1994;98:431–40

88. Fame RM, Chang JT, Hong A, et al. Directional cerebrospinal fluid movement between brain ventricles in larval zebrafish. Fluids Barriers CNS 2016;13:11

89. Worthington WC, Jr, Cathcart RSI. Ciliary currents on ependymal surfaces. Ann NY Acad Sci 1966;130:944–50

90. Greenstone M, Cole PJ. Ciliary function in health and disease. Br J Dis Chest 1985;79:9–26

91. Afzelius BA. Cilia-related diseases. J Pathol 2004;204:470–7

92. Worthington WC, Jr, Cathcart RS. 3rd. Ependymal cilia: distribution and activity in the adult human brain. Science 1963;139:221–2

93. Wagshul ME, Eide PK, Madsen JR. The pulsating brain: A review of experimental and clinical studies of intracranial pulsatility. Fluids Barriers CNS 2011;8:5

94. Malik S, Vinukonda G, Vose LR, et al. Neurogenesis continues in the third trimester of pregnancy and is suppressed by premature birth. J Neurosci 2013;33:411–23

95. Bolisetty S, Dhawan A, Abdel-Latif M, et al. Intraventricular hemorrhage and neurodevelopmental outcomes in extreme preterm infants. Pediatrics 2014;133:55–62

96. Del Bigio MR. Cell proliferation in human ganglionic eminence and suppression after prematurity-associated haemorrhage. Brain 2011;134:1344–61

97. Sarnat HB. Ependymal reactions to injury. A review. J Neuropathol Exp Neurol 1995;54:1–15